AIAA 96-2191
Laminar-Turbulent Transition Research in the Purdue Mach-4 Quiet-Flow Ludwieg Tube

Steven P. Schneider, Steven H. Collicott,
J.D. Schmisseur, Dale Ladoon,
Laura A. Randall, Scott E. Munro,
and T.R. Salyer
School of Aeronautics and Astronautics
Purdue University
West Lafayette, IN 47907-1282

19th AIAA Advanced Measurement and Ground Testing Technology Conference
June 17-20, 1996 / New Orleans, LA

Laminar-Turbulent Transition Research in the Purdue Mach-4 Quiet-Flow Ludwieg Tube

Steven P. Schneider*, Steven H. Collicott†, J.D. Schmisseur‡, Dale Ladoon§,
Laura A. Randall¶, Scott E. Munro‖, and T.R. Salyer**
School of Aeronautics and Astronautics
Purdue University
West Lafayette, IN 47907-1282

Abstract

Simulation and control of high-speed laminar-turbulent transition will only be reliable when it is based on an understanding of the mechanisms underlying the transition process. Measurements of these instability mechanisms are extremely scarce due to the difficulty of constructing the required apparatus. Drawing on the successful 25-year effort at NASA Langley, a low-cost short-duration quiet-flow Mach-4 Ludwieg tube was constructed at Purdue in 1992-93. Controlled perturbations are now being introduced both in the freestream (using a pulsed laser) and on the model surface (using a glow discharge). Measurements are being made with hot-wires, surface hot-film arrays, and laser differential interferometry. Test model geometries include an elliptic cross-section cone, a hemispherical nosetip, a forward-facing cavity, and a scramjet-inlet forebody. The status of this experimental effort is summarized.

Introduction

Laminar-turbulent transition in high-speed boundary layers is important for prediction and control of heat transfer, skin friction, and other boundary layer properties. However, the mechanisms leading to transition are still poorly understood, even in low-noise environments. This difficulty led the Defense Science Board to find that boundary-layer transition on the National Aerospace Plane could not be determined with sufficient accuracy to justify construction of a demonstrator vehicle [5]. Other applications hindered by this lack of understanding include the proposed High Speed Civil Transport [48], high-speed missiles ([24], [29]), and high-speed reconnaissance aircraft [66].

The transition process is initiated through the growth and development of disturbances originating on the body or in the freestream. Environmental disturbances include atmospheric turbulence, entropy spottiness, particulates, and electrostatic discharges [7]. The receptivity mechanisms by which the disturbances enter a boundary layer are influenced by roughness, waviness, bluntness, curvature, Mach number, and so on. The growth of the disturbances is determined by the instabilities of the boundary layer. These instabilities are in turn affected by all the factors determining the mean boundary layer flow, including Mach number, transverse and streamwise curvature, pressure gradient, and temperature [52]. Relevant instabilities include the concave-wall Görtler instability [18], the first and second mode TS-like instability waves described by Mack [42], and the 3D crossflow instability [51]. The first appearance of turbulence is associated with the breakdown of the instability waves, which is determined by various secondary instabilities [21]. Local spots of turbulence grow downstream through an intermittently-turbulent region whose length is dependent on the local flow conditions and on the rate at which spots are generated [47]. Only after the turbulent boundary layer has become fully developed does it appear to become independent of the precise mechanism by which it was formed [27].

In view of the dozens of parameters influencing transition, classical attempts to correlate the general transition 'point' with one or two parameters such as Reynolds number and Mach number can only work for cases that are similar to those previously tested.

*Associate Professor. Member, AIAA.
†Associate Professor. Senior Member, AIAA.
‡Graduate Research Assistant. Member, AIAA.
§Graduate Research Assistant. Member, AIAA.
¶Graduate Research Assistant. Member, AIAA.
‖Graduate Research Assistant.
**Graduate Research Assistant. Member, AIAA.

However, the outlook for reliable estimation methods is more promising than for complex turbulent flows. Correlations between transition and the integrated growth of the linear instability waves have shown promising agreement with experiment [52]. Although these e^N correlations neglect all receptivity and secondary instability effects, they work fairly well for a variety of conditions where the environmental noise is generally low. This may be due to the general similarity of many experiments in terms of roughness, waviness, and environmental noise. In addition, the very rapid growth of instability waves that is common near the onset of transition allows substantial uncertainties in instability-wave amplitude to correlate to much smaller uncertainties in the streamwise location of transition.

Improvements in techniques for estimating the location and extent of transition will depend on improvements in our understanding of the physical mechanisms involved. Direct simulations of transition [28] and the recently developed Parabolized Stability Equations [22, 23] have advanced theoretical-numerical work far ahead of the experimental database. Experimental work that describes not only the location of transition but also the mechanisms involved is needed in order to improve these modern theories.

Unambiguous progress in characterizing the mechanisms of low-speed transition has been made through the use of low-noise wind tunnels with disturbance levels comparable to those in flight, and the study of the development of controlled perturbations. In contrast, the interpretation of most high-speed experiments has been ambiguous due to:

1. Operation in high-noise wind tunnels with disturbance levels much larger than those in flight. The mechanisms of transition operational in small-disturbance environments can be changed or bypassed altogether in high-noise environments. Figure 23 in reference [15] shows rms static-pressure fluctuations in flight and in the lowest-noise supersonic wind tunnels. At Mach 3, the noise levels of the quietest conventional tunnels are still about 4 times greater than the best available flight data (which may itself be dominated by instrument noise). Figure 21 in reference [15] shows that transition Reynolds numbers on a sharp cone at zero angle-of-attack at Mach 2 are 50% higher in flight than in the lowest-noise conventional wind tunnels. Figure 11 in reference [36] shows that the noise radiated from the turbulent boundary layers on the walls of conventional hypersonic wind tunnels increases with the square of the Mach number. This makes the situation much worse for hypersonic facilities [63].

2. A lack of measurements carried out in controlled disturbance environments. Most experimental work has studied natural transition caused by uncontrolled and poorly characterized disturbance fields. However, detailed measurements of unsteady three-dimensional flow fields are only possible when the flow fields are repeatable with respect to a known phase reference. The difficulty of making very sensitive, high-bandwidth measurements in unsteady 3D flows has been exacerbated by the high cost and correspondingly limited availability of the requisite wind tunnels.

These difficulties must be overcome before high-speed transition research can begin to match the maturity characteristic of low-speed work.

Slow progress overcoming the first difficulty has limited work on the second. Only in the last two decades have low-noise supersonic wind tunnels been developed [3, 74]. This development has been difficult, since the test-section wall boundary-layers must be kept laminar in order to avoid high levels of eddy-Mach-wave acoustic radiation from the normally-present turbulent boundary layers. The effects of this acoustic noise are profound. For example, linear instability theory suggests that the transition Reynolds number on a 5 degree half-angle cone should be 0.7 of that on a flat plate, but noisy tunnel data showed that the cone transition Reynolds number was actually higher than the flat plate result. Only when quiet tunnel results were obtained was the theory verified [10]. Consequently, both the location and the parametric trends for transition in conventional wind tunnels can be dramatically different from those in flight. ***Only the study of controlled disturbances in a controlled quiet environment can produce unambiguous data suitable for development of reliable theory.*** Reliable predictive methods will have to be based on estimates of the flight disturbance environment.

The Purdue Quiet-Flow Ludwieg Tube

Introduction

Quiet facilities require low levels of noise in the inviscid flow entering the nozzle through the throat, and laminar boundary layers on the nozzle walls. These features make the noise level in quiet facilities

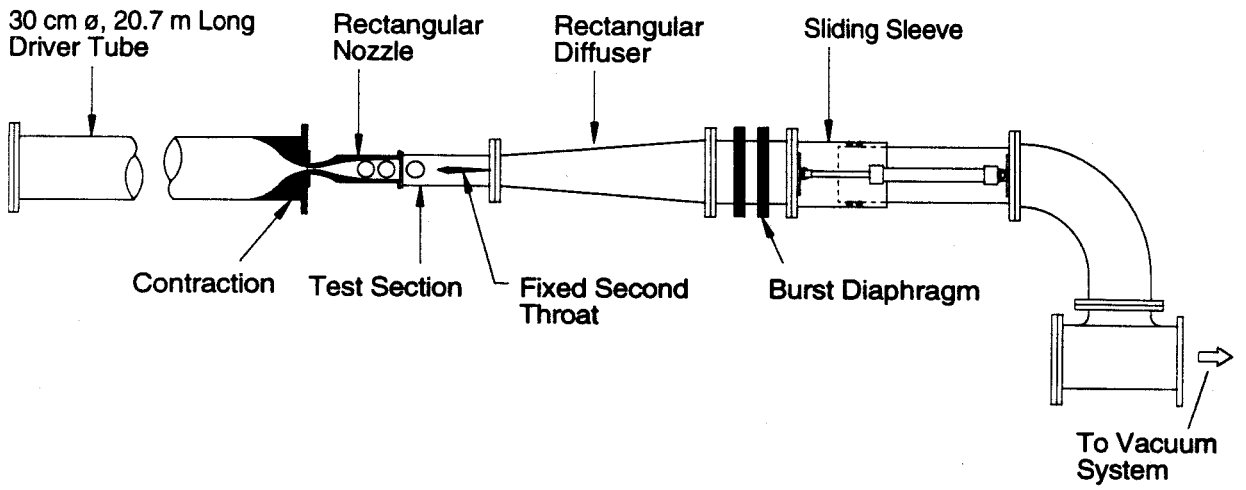

Figure 1: Schematic of Purdue Quiet-Flow Ludwieg Tube

an order of magnitude lower than the 0.5 to 3 percent pressure fluctuations typical of conventional facilities. In order to reach these low noise levels, conventional blow-down facilities must be extensively modified. Requirements include a 1 micron particle filter, a highly polished nozzle with bleed slots for the contraction-wall boundary layer, and a large settling chamber with screens and sintered-mesh plates for noise-reduction [3]. To reach these low noise levels in an affordable way, the Purdue facility has been designed as a Ludwieg tube (see ref. [58], [59], [60], and [61] for details). A Ludwieg tube is a long pipe with a converging-diverging nozzle on the end, from which flow exits into the nozzle, test section, and second throat (see, e.g., Figure 1 and ref. [40]). A diaphragm is placed downstream of the test section. When the diaphragm bursts, a shock wave passes downstream, and an expansion wave travels upstream through the test section into the driver tube. The nominal end of the run occurs when the expansion wave has returned to the test section after reflecting from the upstream end of the driver tube. The large vacuum tank used at Purdue currently allows operating for about 30 cycles of expansion-wave reflection – this provides roughly 30 quasi-steady run segments between which the unit Reynolds number drops about 1% [65]. The actual run duration depends on the stagnation-pressure losses induced by the model, and has varied from less than 0.5 s to about 4 s. This extended runtime allows many shots of a 10-Hz laser during a single run, and in some cases allows observation of transition on a single fixed sensor during the run.

The existing Purdue facility is based on a 30.5-cm diameter driver tube that is 20.7 meters long. Flow is initiated using a burst-diaphragm assembly located downstream of the test section. A smooth contraction tapers from the driver tube to the first throat, which is followed by the 9.7x10.9 cm Mach-4 rectangular nozzle. Figure 2 shows the nozzle, which was fabricated at NASA Langley in the middle 1970's according to a conventional design. The lines drawn upstream from the exit of the nozzle show the approximate beginning of the uniform-flow region. These lines are drawn at the Mach angle for Mach 4. Also shown on the figure is a schematic of the region affected by the onset of turbulence in the boundary layers on the tunnel walls. The test rhombus between the beginning of uniform flow and the region affected by turbulence on the tunnel walls is characterized by quiet uniform flow. The axial length of this quiet uniform flow region is labeled L_q in the figure, and is used to form the quiet-flow Reynolds number.

Quiet-flow operation to length Reynolds numbers in excess of 400,000 at unit Reynolds numbers of about 40,000 per cm has been demonstrated using pitot-pressure measurements carried out on the centerline of the facility. Pitot pressure fluctuations of about 0.07 percent of the mean pitot pressure were considered borderline quiet, since these corresponded to the presence of high-noise turbulent-spot signatures in about 1 percent of the run duration. Details regarding these experiments can be found in references [61] and [58]. Since $q/P_t = 0.074$ and $P/P_t = 0.0066$ at Mach 4 [70], and $P'_{rms}/P_{mean} \simeq 1.08 P'_{t,rms}/P_{t,mean}$ [4], $P'_{t,rms}/P_{t,mean} = 0.0007$ corresponds to $P'/q = 6 \times 10^{-5} = 0.006\%$. Here, q is the dynamic pressure, P_t is the total pressure, P is the static pressure, a prime denotes the fluctuation signal (with the mean subtracted), and subscripts of 'rms' and 'mean' denote the rms and mean values

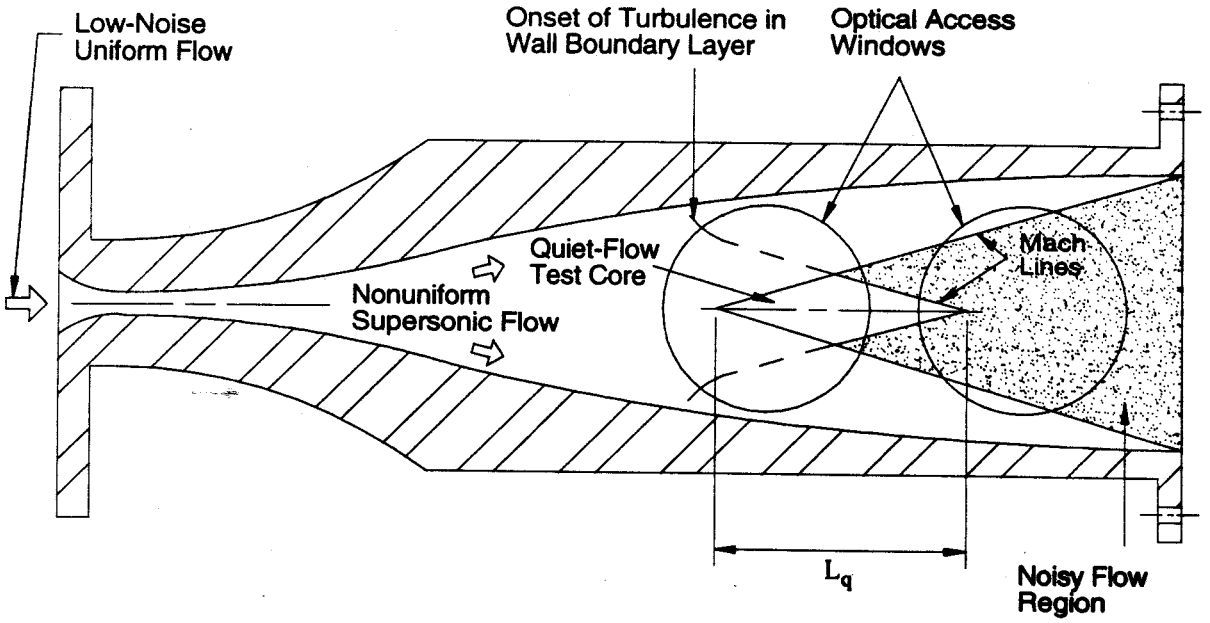

Figure 2: Schematic of Mach 4 Quiet-Flow Nozzle

of the quantity. This places the quiet-tunnel data a factor of 5 lower than the lowest flight data in Figure 23 of [15], even though the flight data is bandlimited to about 10kHz. This suggests that the flight 'noise' data in reference [15] is substantially increased by electronic noise.

Quiet-flow operation at these Reynolds numbers makes the facility suitable for measurements of receptivity and instability, but not complete transition to turbulence. These quiet-flow results also show that the basic concept for the facility is sound. Operation with quiet-flow at higher Reynolds numbers now requires only a larger and higher quality test section.

Summary of Recent Facility Improvements

Several major improvements have been made to the facility since summer 1994. The most important is a new burst-diaphragm apparatus. A double-diaphragm technique was originally used. Two 0.002-0.004-inch Mylar diaphragms were held by two Tube-Turns quick-opening flanges. The Tube-Turns clamps are part of the wind tunnel. Unfortunately, the flanges had to be aligned to within a few thousandths of an inch in order to squeeze the Mylar uniformly so that it would not slip out on one side and cause premature rupture.

The new burst-diaphragm apparatus is shown in Figure 3. A pair of precision-machined steel rings is used to hold the diaphragm. The rings are attached to a sheet-steel ring that is held by one of the original Tube-Turns clamps. In this way, the clamp

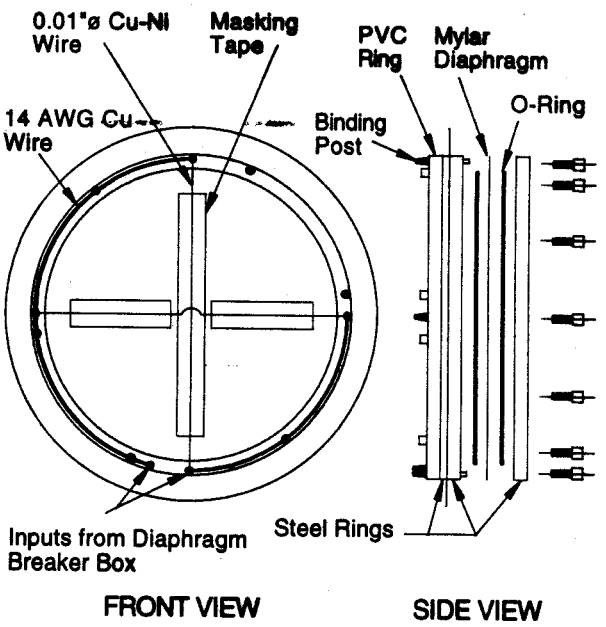

Figure 3: Burst Diaphragm Apparatus

is thereby required only to seal the steel ring, and not to evenly squeeze the Mylar. Small nichrome wires are taped to the single diaphragm in a cross pattern, using masking tape. The Nichrome wires are connected to a pulsed-heating apparatus consisting of 0.76F of 40V capacitors that are discharged through a high power SCR (International Rectifier ST230S16P0). The leads are wired through binding posts on a PVC ring to allow easy diaphragm changes. The 20A of current discharged through the typical 2 ohm load heats the wires (sometimes red-hot), melts the Mylar, petals the diaphragm, and initiates the flow. Flow is thus initiated by flicking a switch. Although it is also possible to initiate the current-pulse using the synch-out from the 10-Hz laser, synchronization of the flow and laser is still limited, due to residual scatter (on the order of 0.1s) in the diaphragm-breaking process. The new apparatus has been used for hundreds of runs in the 10-25 psi pressure range, primarily with 0.007 and 0.010-inch Mylar (12-inch diameter). The method is economical and highly reliable.

A second improvement was to the tunnel-support apparatus, originally consisting of a single overhead I-beam from which the components were suspended using turnbuckles and trolleys. Figure 1 sketches how the nozzle and test-section must be disconnected and moved apart in order to change models. The hydraulically-operated sliding sleeve is used to move the two sections apart for access. Unfortunately, the single vertical support did not maintain horizontal alignment during the opening and closing process, so tunnel alignment was often a problem. A new support structure consisting of a pair of overhead I-beams was therefore constructed, each angled 22-degrees from vertical. Two slanted turnbuckles now support each section, allowing control of both vertical and horizontal position. Control of rotation remains to be effected, using special fittings at the turnbuckle-attachment points.

Since the original sliding sleeve only allowed opening the tunnel about 4 inches, model changes were difficult. The third improvement was to construct a new sliding sleeve with a 32-inch range of motion. A second surplus vacuum pump was also installed, thereby increasing pump rate from 140 cfm to 270 cfm, reducing pump-down time from about 30 minutes to about 15, and allowing redundancy for maintenance. Finally, the whole area has been enclosed and air-conditioned; this was essential for repeatable operation of the Nd:YAG laser used in the laser-spot experiments described below.

Run-time Drop in Pressure and Temperature

During the 3-4 second run of the facility, the stagnation pressure (inferred from pitot pressure measurements) drops about 9 percent per second [65]. Published theories for the stagnation pressure drops in Ludwieg tubes grossly underestimate this reduction, giving rise to concerns about our ability to predict the performance of the facility when operated with a new test section. For example, the expansion wave returns to the test section about 0.12 s after reflecting from the upstream end of the 68 ft. driver tube. At this time, the pressure has dropped about 0.5%. The major theories for computing the pressure drop in Ludwieg tubes were developed for facilities with higher driver-tube Mach number, and are based on analyses of the stagnation pressure losses caused by the expansion wave and the buildup of boundary layer on the wall of the driver tube [49, 54]. For our tube radius of 6 in., and our 3.8 by 4.3 in. Mach-4 test section, the driver-tube Mach number is about 0.008, and the tube velocity is about 2.8 m/s. According to reference [72], the stagnation pressure drops from 14.7 psia to 14.54 psia across the driver-tube expansion wave (about a 1% change); this weak change should remain constant as the wave travels down the tube. Following Russell et al. [54], the pressure drop due to boundary-layer growth after 0.12 s would be 0.002%, following Piltz [49], the drop would be 0.007%; both of these values are two orders of magnitude below the observed value of 0.5%.

It appears that our low driver-tube Mach number has somehow invalidated the assumptions in these theories. Fortunately, we have recently discovered a very simple model that fits our data well. The flow out of the driver tube is simply modeled as an isentropic expansion from a reservoir through a choked nozzle, with the massflow set by the stagnation pressure P_t and the stagnation temperature T_t. The isentropic assumption carries an assumption of zero heat transfer with it, which is reasonable given the short runtime. Using Fliegner's formula [67, eqn. 4.18], the massflow can be expressed as

$$V\frac{d\rho_t}{dt} = -A^*\frac{P_t}{\sqrt{RT_t}}c_1, \qquad (1)$$

where ρ_t is the driver-tube density, V is the driver-tube volume, A^* is the throat area, R is the gas constant for air, and

$$c_1 = \sqrt{\gamma\left(\frac{2}{\gamma+1}\right)^{\frac{\gamma+1}{\gamma-1}}}. \qquad (2)$$

For an isentropic perfect gas,

$$\frac{P_t}{P_{t,i}} = \left(\frac{\rho_t}{\rho_{t,i}}\right)^{\gamma}, \tag{3}$$

where $P_{t,i}$ is the initial driver pressure and $\rho_{t,i}$ is the initial driver density. This simple pair of equations can be combined with the perfect-gas relation and solved to yield

$$\frac{P_t}{P_{t,i}} = \left[1 + \frac{\gamma - 1}{2}\frac{A^*}{V}\sqrt{RT_{t,i}}tc_1\right]^{\frac{2\gamma}{1-\gamma}}, \tag{4}$$

where t is the time from flow initiation and $T_{t,i}$ is the initial driver temperature. Using the isentropic relations, the stagnation temperature variation is

$$\frac{T_t}{T_{t,i}} = \left[\frac{P_t}{P_{t,i}}\right]^{\frac{\gamma-1}{\gamma}}. \tag{5}$$

Experimental data has been obtained using Kulite XCQ-062 pressure transducers operated in a pitot mode, as in our other experiments. The DC output is sampled at 50kHz using LeCroy 9304AM oscilloscopes, and the 5-second 250 kpt records were smoothed by averaging blocks of 50 points. The pitot pressure was converted to stagnation pressure using the 0.1388 ratio of stagnation pressures across a normal shock at Mach 4. Since the time of flow initiation is obscured by the flow startup, the timing of the experimental data was fitted to the isentropic formula at a pressure ratio of 0.85 (after the startup is well complete). The results are shown in Figure 4. The isentropic theory (equation 4) is plotted, along with 4 sets of experimental data. Although the two runs obtained at 14.5 psia repeat fairly closely, there are small residual differences that have yet to be explained. The higher-pressure run at an initial driver pressure of 18.2 psia is a bit above the theoretical curve, while the lower-pressure run is somewhat below. The agreement is more than sufficient for design studies. The authors await a detailed explanation for why this simple theory works well when the more sophisticated models do not.

The temperature variation is compared in Figure 5. Here, the stagnation temperature in the flow is measured with a 3.8-micron diameter tungsten wire, using a small 2.5 mA current to sense the resistance variations. A REF01 integrated circuit is

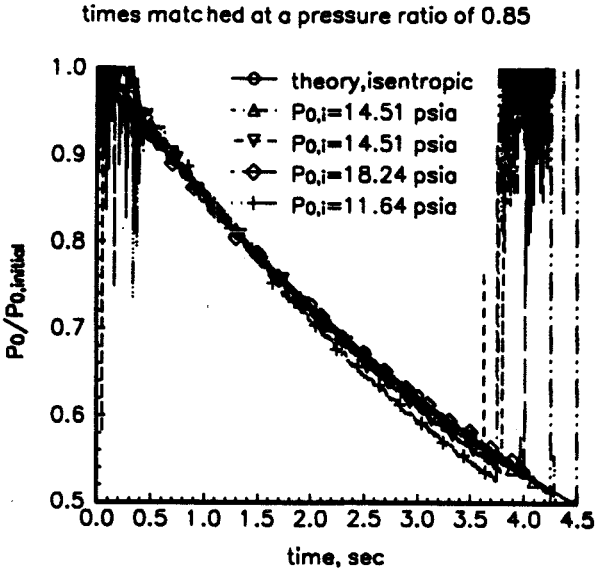

Figure 4: Stagnation-Pressure Measurements

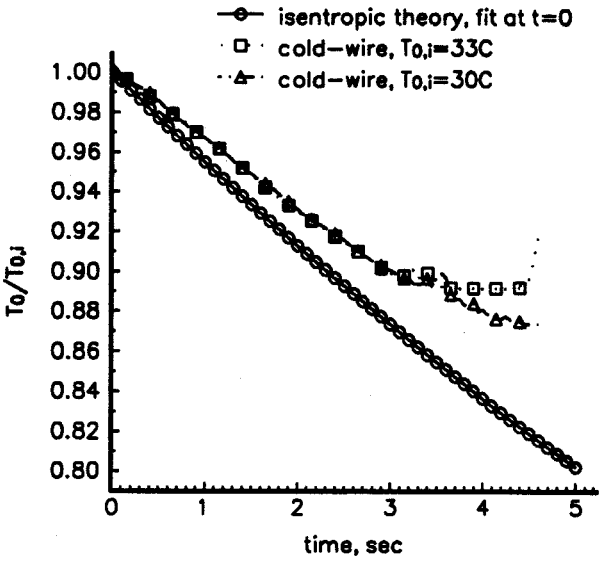

Figure 5: Stagnation-Temperature Measurements

used to supply 10V to a 4020-ohm ballast resistor in series with the hot-wire; the hot-wire output is amplified with an INA103 integrated circuit before digitization by the scope. The data are again digitized at 50kHz using LeCroy 9304AM scopes; the resulting 250 kpts are averaged in groups of 2500 to yield 100 points over 5 seconds. The wires were oven-calibrated to determine the resistivity coefficient. An empirical recovery factor of 0.96 is used to correct the measurements to stagnation temperature [37, p. 174-75]. The two cold-wire runs repeat well, until near the end of the run. Although both are significantly above the simple theory, it remains useful for design purposes. This cold-driver data was obtained after a set of hot-driver runs; it may be that the cooling to room temperature was somehow incomplete.

Need for Driver-Tube Heating

In order to study flows more similar to the hypersonic flows of Air Force interest, a quiet-flow nozzle that operates at higher Mach number is needed. The second-mode instability, characteristic of hypersonic conditions, begins to become effective on cones and flat plates at Mach numbers between 5 and 6 [42]. Transition estimates based on e^N theory for a wall at 70% of the adiabatic wall temperature show that the second mode begins to dominate transition for a round cone at zero AOA at about Mach 5 [43, Fig. 9]. The second mode is clearly dominant under cold-wall conditions at Mach 6 [43, Fig. 10], although it takes until Mach 7 for it to dominate under adiabatic-wall conditions. This theoretical result has experimental support [71]. Since most hypersonic vehicles are operated with wall cooling, and our facility has a short runtime, operation at Mach 6 with a stagnation temperature of 450K and a model wall temperature of 245K appears to be a reasonable plan. The simplest operation will be with a stagnation temperature of 450K (just at the static liquefaction limit) and the model at room temperature (about 300K), where the second mode will probably still dominate the highly symmetrical zero-AOA cone flow.

Mach number affects not only this second mode. Tests of 3 symmetric-flow cases in conventional wind tunnels showed that the square root of the critical roughness Reynolds number jumps by a factor of 10 between Mach 4 and Mach 5 [6, Figure 8]. This is only a striking example of the well-known fact that it is very difficult to trip a hypersonic laminar boundary layer, presumably because most of the massflow is relatively far from the wall. Mach 6 will clearly be high enough to study many of these kinds of effects.

Although Mach 6 is in the low range of hypersonic conditions, tunnel construction, operation, and instrumentation costs increase dramatically between Mach 6 and Mach 8, and in any case NASA Langley already has a major effort at Mach 8 [74]. It would be highly desirable to maintain quiet flow to truly hot hypersonic conditions, where dissociation and ionization occur, but the only paths that even seem remotely possible are highly uncertain and expensive [17]. Note that transition Reynolds numbers are about 2-3 million on near-sharp 5-degree half-angle cones in the free-piston hypersonic T5 facility [25]. These values are much less than the 20 million reported for the Re-Entry F data [75], probably because of the high levels of noise in T5, although bluntness or some other factor could also be involved.

Plans thus call for construction of a high-Reynolds number quiet-flow nozzle for operation at Mach 6. However, it is necessary to heat the driver-tube air in order to avoid test-section condensation at Mach 6. Although some supercooling may well be possible, a conservative heating design will allow a driver-tube temperature of about 450K (the static liquefaction limit [73]).

Measurements with Heated Driver-Tube Air

Therefore, apparatus for heating the driver tube has been constructed and is currently being tested with the existing Mach-4 test section. The effect of heating on the extent of quiet flow is of particular interest (cf. references [14], [20, Figure 10], [44]). Although noise measurements are not yet available, preliminary data on the heating apparatus and effects are presented here.

The main part of the heater apparatus is a system for heating the 12-inch carbon steel driver tube, which is 0.375-inch-wall standard weight pipe. The paint on the pipe is rated for operation at 600F and the pipe is rated for 200 psi at 400F. The epoxy used to smooth the joints is unofficially rated for operation at 600F. The initial plan for heating the pipe called for passing a current directly through the pipe as is done at the DLR in Germany [39], where a 3000 amp 22V supply is used. However, such a high-current low-voltage supply was not readily available in our lab. Instead, a pair of existing 200A 30V DC supplies are used. In order to match the resistance of the heating elements to these supplies, 16AWG copper wire is wrapped around the pipe in a spiral with a 2-inch spacing between coils. The pipe is electrically insulated from the wire using fiberglas cloth. Four parallel lengths of wire are cur-

rently used, with a single supply, to heat the downstream half of the driver tube. The wire-wrapped pipe is then insulated with 4-inch fiberglas pipe insulation. A separate heater was developed to add heat at the downstream end of the driver, since the heat conducting away through the test section otherwise makes achievement of a uniform driver temperature impossible. Although the nozzle and test section are warmed by the stray conducted heat, they remain relatively cool, easing operations. The actual runtime is so short that runtime heating of the nozzle is negligable.

The major issue in the design of the heating system was achieving uniformity in the temperature of the driver tube and gas. It appears critical that no convection currents be present in the gas when it is accelerated into the test section during the run, or noise may be generated. The driver tube is thus instrumented with a total of 28 thermocouples placed around the pipe at six streamwise stations, 0, 3, 6, 10, 13, and 18 feet upstream of the nozzle throat. Any four of these can be monitored at one time using a switching system. The ungrounded thermocouples are placed directly on the pipe, under the fiberglas cloth.

Although plans initially called for heating the entire driver, only the gas from the downstream end of the driver ever actually makes it into the test section during the run (with a 4-second run and a 2.8 m/s driver velocity, only the first 11.2 m of gas enters the test section). Currently the last 25 feet of the driver are heated, and an additional 3 feet is insulated. It takes about 3-4 hours to heat the driver tube to 100-120C. Somewhat surprisingly, it also takes more than 4 hours for an already-hot driver tube to heat a new charge of air. To overcome this turnaround-time problem, a 4.5kW off-the-shelf 'circulation heater' has been installed in the compressed-air line to the driver, downstream of the original particle filter. This should allow charging the driver with air that is already hot, reducing the time required for the driver and air to reach equilibrium. A second particle filter was added downstream of this heater to remove 99.95% of particles above 0.6μ. This off-the-shelf high-temperature filter is rated to 450F.

Measurements of the stagnation temperature are made during the run with a 3.8 micron tungsten hot-wire operated in temperature-sensing mode as described above. The output of the constant-current anemometer is digitized at 25kHz using the LeCroy 9304AM scopes; segments of 2500 pts were then averaged to produce Figure 6, which shows the stagnation temperature in the driver tube as a function of

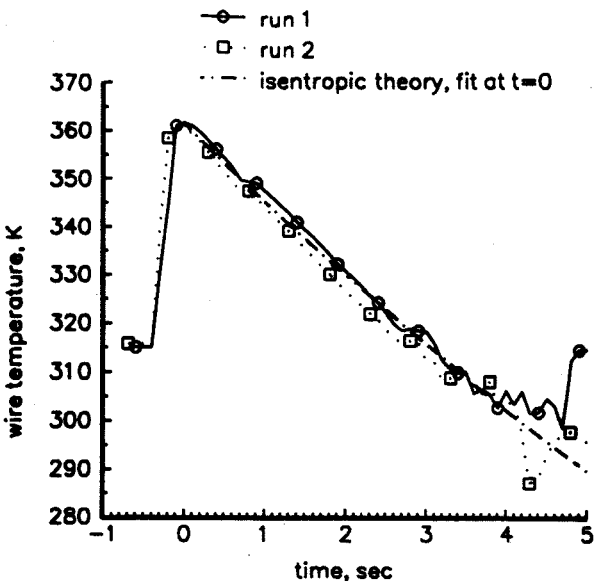

Figure 6: Stagnation Temperature Records

time for two runs. In each case, the run began about 3 hours after the tube was charged. Since the beginning of the run is obscured by startup processes, the experimental data is shifted so that $t = 0$ at the peak. The isentropic theory (equation 5) is also plotted; the peak experimental temperature is used to normalize the theory. Although the thermocouples on the driver tube read 373K on average, the peak temperature inferred from the cold wire was 361K. This difference may be due to calibration errors. The good fit to the simple theory suggests that the decay of the stagnation temperature during the run is not due to nonuniformities in the heating, as was first supposed; it is rather a simple consequence of the isentropic expansion of the driver gas. It is not yet clear why this hot-driver data fits the isentropic temperature-drop curve better than the cold-driver data in Figure 5; the difference there is likely to be due to flaws in experimental procedure.

Instrumentation for Introducing Controlled Perturbations

Laser-Generation of Hotspots in Freestream

If a local perturbation can be generated in the freestream of a supersonic flow, then the evolution of a local disturbance that passes through the shock and into the boundary layer can be studied. Packets of instability waves will presumably be generated, in a fashion somewhat similar to the work of Gaster at

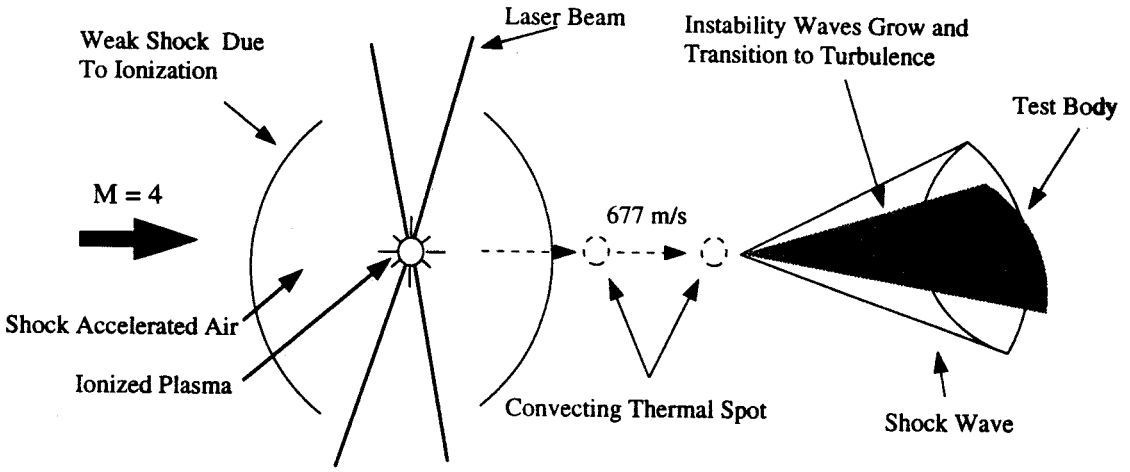

Figure 7: Schematic of Laser-perturbation Application

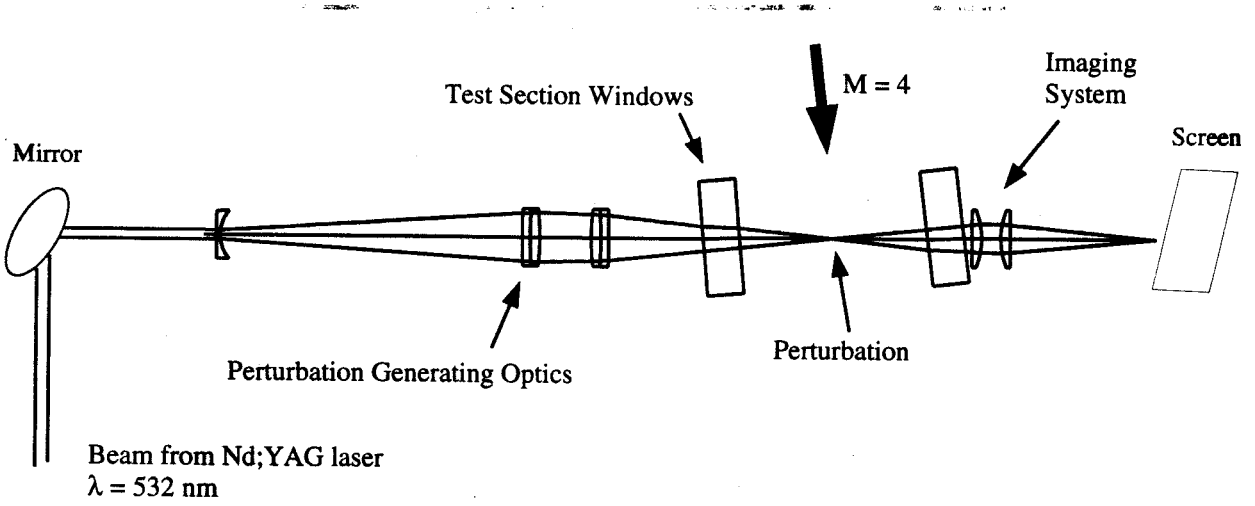

Figure 8: Optical System for Generating Perturbations

low speeds [19]. A method has been developed for generating repeatable, localized, controlled perturbations by photoionizing air using a pulsed laser. Characterization of the perturbation is ongoing in the Mach 4 low-noise environment of the Purdue University Quiet-Flow Ludwieg Tube. Further details can be found in reference [55].

The photoionization effected at the laser focus is described in reference [77]. The initial disturbance consists of a plasma core surrounded by a region of non-ionized air and the shock wave produced during ionization. After the end of the laser pulse, the plasma core relaxes and remains as a region of hot recombined gas, referred to as the thermal spot. The thermal spot convects with the local velocity of the flowfield and forms the portion of the disturbance useful as a local perturbation. For example, Figure 7 shows a schematic of the perturbation incident on an elliptic-cone model, where it is being used for receptivity measurements. The shock wave weakens and approaches a spherical shape with increasing distance from the plasma core [62]. In Mach 4 experiments at about 1 atm. total pressure, the shock wave is too weak to be observed at a hot wire 15 mm away from the focus. The formation of the disturbance depends on the intensity (average power per unit area in the focal region) of the laser pulse. Thus, both the energy in the laser pulse and the size of the focus affect the ionization process. A minimum intensity, known as the threshold intensity, is required to initiate ionization. Once the intensity threshold for the onset of ionization has been surpassed, increasing intensity results in increasingly strong perturbations [55, 62]

A 10-Hz frequency-doubled Nd:YAG laser is used. An injection-seeded laser must be used to obtain reasonable repeatability [62]. The pulse duration is approximately 7 ns with a maximum pulse energy near 260 mJ. A schematic of the optical system is shown in Figure 8. To prevent back reflections off the test section windows from damaging optics, the focusing beam is tilted 5 degrees from the window normal. The tilt increases aberrations, but not sufficiently to hinder system performance. Initially, difficulty was encountered in maintaining the position of the perturbation within the test section. Since the Ludwieg Tube is subject to axial forces (i.e. recoil and vacuum forces) during the operation of the facility, the optical system, which is bolted to the test section, occasionally shifts by several millimeters with respect to the laser beam. Adjusting the mirrors to recenter the beam in the lenses changes the position of the perturbation. This problem is alleviated by imaging the perturbation as the beam

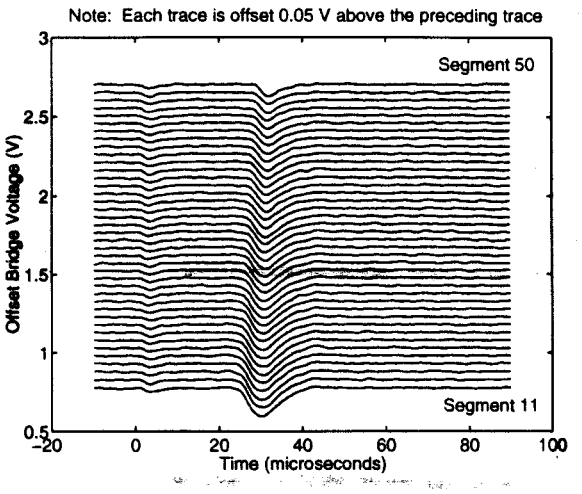

Figure 9: Laser-Spots Passing Hot-Wire in a Single Run

passes out of the test section. The perturbation location is repeatable inside the test section by adjusting the spot-generating optics before the run so that the image of the perturbation is at a fixed position on a screen outside the test section.

Measurements of the convecting thermal spot have been made with a constant temperature anemometer (CTA), the TSI IFA 100, using the standard bridge with no signal conditioning. The hot-wire sensing element is a 0.0038-mm diameter tungsten wire mounted between two 0.076-mm dia. needles spaced 0.51 mm apart. The typical frequency response of the wire is about 120 kHz, operating at an overheat ratio of approximately 1.7. The sting-mounted hot-wire probes are positioned in the flowfield with a traverse which allows the sensor to be moved both vertically and in the streamwise direction along the transverse centerline of the test section. The output bridge voltage is sampled in both continuous and segmented data records using LeCroy 9304AM digital oscilloscopes. The continuous data records contain 250,000 points sampled between 50 and 250 kHz while the segmented records consist of 50 segments of 5,000 points sampled at rates between 1 and 10 MHz. Each segment in the segmented data sets is triggered from the synch pulse generated by the laser Q-switch circuit.

The entire set of segments collected during the quiet portion of a single run is plotted in Figure 9. Due to pre-triggering of the oscilloscope the first segment collected after flow was initiated is segment number 11. The stagnation pressure was about 99 kPA and the stagnation temperature was about 22-24C, while the laser energy was about 227 mJ per

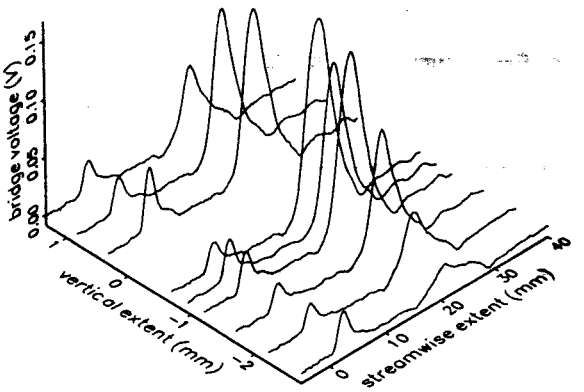

Figure 10: Vertical Extent of Laser-Spot

pulse, and the measurement was made about 15 mm downstream of the focus of the laser. In each trace, the pulse at $t \simeq 0$ is electromagnetic noise radiated from the plasma formed during the laser pulse, and the pulse at $t \simeq 30$ is the heated region passing the hot-wire. The pulse is negative, for less current is needed to maintain the hot-wire at constant temperture inside the thermal spot. As seen in Figure 9, the thermal spot is consistently formed with every laser pulse until the end of the data acquisition. Note that the amplitude of the CTA response decreases during the run. This amplitude attenuation is presumed to be due to a reduction in the energy transferred from the laser to the gas as the freestream density decreases during the run. For some runs the spot is not formed in the last few segments of the run as the freestream density drops below the threshold required for ionization. Although the CTA response to individual thermal spots varies by 5-10%, presumably due to shot-to-shot variations in the laser, the average response over the first ten thermal-spot passages is fairly consistent for similar driver tube conditions and laser pulse energies. Calculation of the thermal spot convection velocity using the time to peak bridge response at several streamwise locations indicates that the perturbation moves at the facility freestream velocity, about 680 m/s.

By vertically traversing the hot wire the profile of the convecting thermal spot has been determined. Three-dimensional plots of the averaged response of the hot-wire to the first ten thermal spot passages are shown in Figure 10 for multiple vertical locations 15 mm downstream from the spot origin. The sign of the voltage has been changed to facilitate viewing the traces. All data in the figure were collected at ambient driver tube conditions ($P \simeq 98.6$ kPa, $T = 21 - 27$ C) with the laser pulse energy between 220 and 225 mJ per pulse. Using the convection velocity of 677 m/s, the time signal has been transformed to a length scale. The vertical dimension is the distance from the approximate spot center.

The data show that the spot is repeatable to within about 10%, is about 5 mm in diameter, and grows in size only very slowly with streamwise distance [55]. Calibrated measurements of the thermal spot have been attempted using high-overheat constant-temperature anemometry, but the temperature fluctuations in the spot are apparently too high to get reasonable massflow-fluctuation values this way. Cold-wire technique does not have enough frequency response to measure these temperature fluctuations. Calibrated results will require either mode-diagram hot-wire work, or differential interferometry (see below).

Local Surface Glow-Discharge Perturber

Local perturbations are also being generated at the surface of the model. A glow-discharge perturber developed from those used at ITAM in Novosibirsk, Russia is being used [65, 30]. These perturbations may generate a harmonic point source, wave packets, and turbulent spots, allowing detailed characterization of all three.

To date, preliminary bench and wind tunnel tests have been conducted in order to characterize the glow, gain some familiarity with the glow circuit, and to address other electronics issues [34, 35]. Both the glow-discharge electronics and the perturber components were custom built at Purdue University. Figure 11 shows the glow electrode installed in the elliptic cone. The electrode design and glow-discharge circuit were developed from those used by Kosinov et al. [31, 30].

Bench tests show that a glow discharge can be achieved for frequencies up to 350 kHz. This limit is set by the electronics of the circuit. Recent wind-tunnel tests have demonstrated that a stable glow can be established and maintained during the startup and run of the Ludwieg tube. The glow can also be modulated. Consequently, the device can be used to create wave packets. Wind-tunnel tests have been conducted in which the glow frequency was varied by sweeping the input frequency over a 10 kHz range for intervals of 100 msec, since sweeping the input frequency is an efficient means of identifying those which are most unstable.

To maintain a stable glow during Mach 4 flow,

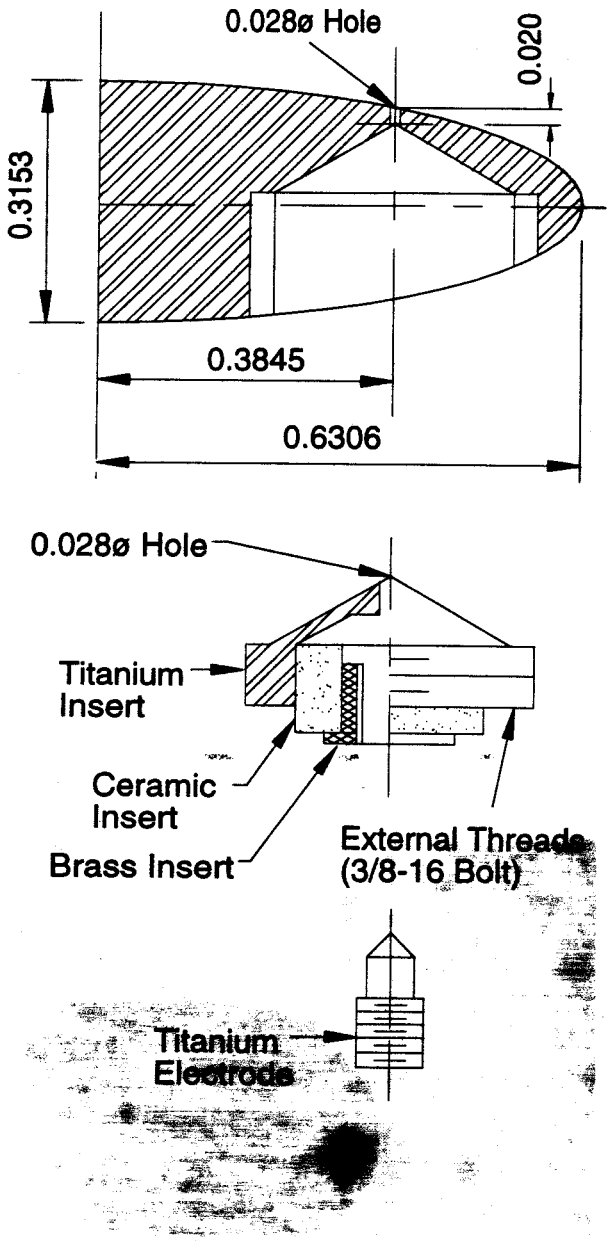

Figure 11: Drawing of Glow-Discharge Perturber in Cone. Dimensions in Inches. Scale: 4:1.

the current-limiting ballast resistor, electrode spacing, and input voltage values must be selected carefully, for a given input frequency, to avoid arcs or spikes. The arcs are unacceptable for many purposes, since the noise emitted completely obscures the signals from the hot-film sensors. Also, the wires leading from the glow electronics to the electrodes must be shielded from those of the hot-films to avoid electro-magnetic coupling. Experiments aimed at generating turbulent spots on the elliptic cone model are currently in progress.

Measurement Instrumentation

The problem of measuring instability waves in hypersonic boundary layers is discussed in detail in reference [12]. Traditional constant-temperature hot-wire technique is currently being used, both in the freestream and in the boundary layer [55]. Arrays of surface hot-films are useful for determining whether the surface flow is laminar or turbulent. Since a continuous signal is obtained, it is possible to study the passage of turbulent spots, as well as the average intermittency, or fraction of time that the flow is turbulent. The technique was demonstrated using measurements carried out on the tunnel wall [56]. Arrays of this type have now been fabricated for an elliptic cross-section cone and a scramjet-inlet model (see below). Improved anemometers are being constructed to allow DC-coupled measurements of the weak hot-film signal; the intermittency of these DC-coupled data can be determined less ambiguously by using a PDF technique [57]. It should be possible to operate 8-12 channels simultaneously by the end of summer 1996.

High-Sensitivity Differential Interferometry

High-sensitivity single-point differential interferometry capable of resolving optical pathlength differences of $\lambda/1000$ with a signal-to-noise ratio of 100 is currently being developed, following Smeets [68] and Azzazy [2]. This technique measures the optical-pathlength difference between two adjacent laser beams, with extreme sensitivity, allowing measurements of density differences integrated along the path of a narrow beam that passes through the edge of the boundary layer, where the hypersonic instability-waves have maximum amplitude [12]. The technique is generalizable to linear-array measurements [69], and will be used to measure second-mode waves and other instability phenomena that are aligned nearly perpendicular to the flow. The fluctuation in optical pathlength caused

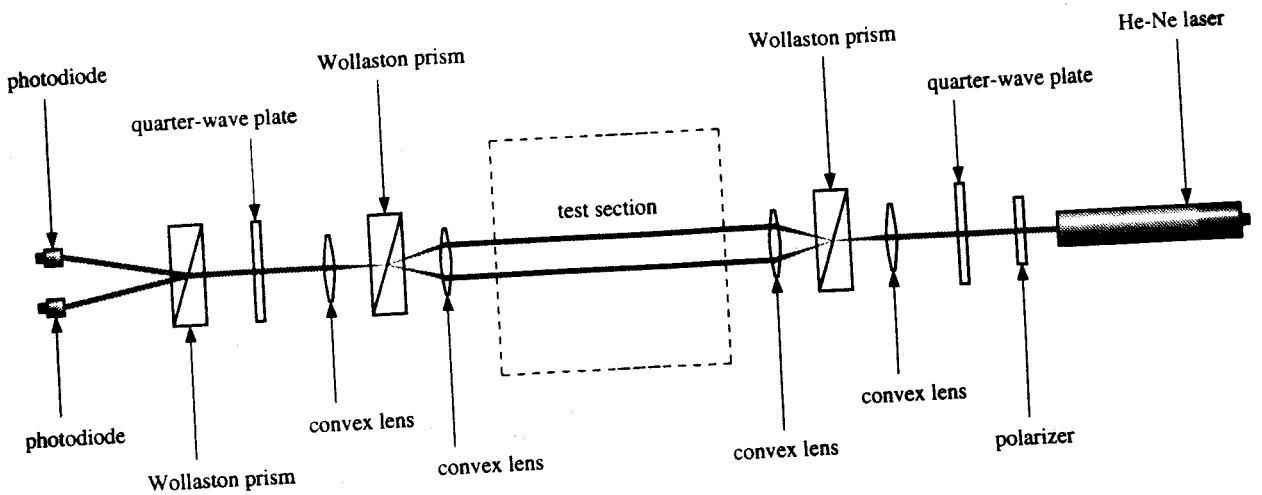

Figure 12: Schematic of Laser Differential Interferometer

by the second-mode waves is estimated to be about 0.002 wavelengths or 1 nm [12, page 8], so this very high sensitivity is necessary. The high bandwidth of this technique (well above 1 MHz is readily feasible) will first be used to resolve the passage of the laser-generated localized perturbations in the freestream. Since these perturbations are 4-5 mm in diameter and are travelling at 670,000 mm/s, very high bandwidth is required to clearly resolve them.

The simplest form of the LDI sends two closely spaced, narrow beams through the test section and interferes them on a photodetector, as shown in Figure 12. From one 1.5 mW stabilized HeNe laser, two beams are formed, and recombined through a series of Wollaston prisms, quarter-wave plates, convex lenses, and a polarizer (if the laser is not already polarized). An additional Wollaston prism splits the recombined beams into two pairs of beams with complementary interferences. The relative change in light intensity due to the interference in the beam pairs is detected with two high-speed photodiodes. After adjusting to the infinite fringe spacing, the phase relation between the interfering beams of each pair corresponds to the linear part of an interference slope between a light and dark band. Small optical path changes by a phase object in the test section lead to light level changes on the photodiodes, and hence electrical signal changes in the photodiode circuitry. Differencing the complementary electrical signals from the two photodiodes across one load resistor creates a signal which is doubled in amplitude, and simultaneously suppresses noise due to laser-light fluctuations. The object in the test section must be imaged onto the photodiodes to avoid any schlieren effects. Spatial density or index of refraction gradients cause light rays to bend and also to be altered in phase. Interferometers function on the second phenomenon, and so the imaging lens is used to negate the the first effect.

The sensitivity and practical signal-to-noise ratios attainable with the current system are nearing those achieved by Smeets. Using a 10 kΩ load resistor and the manufacturers quoted junction capacitance for the high speed PIN photodiodes, an RC time constant of 105 nsec is computed to give an estimated system frequency response of 9.5 MHz. This does not include any cable or input capacitance to the recording device, which will of course reduce the maximum frequency response. Peak-to-peak electrical noise in the circuit is 1.8 mV with an rms of 220 μV. This noise sets the sensitivity limit (signal-to-noise ratio of one) to a minimum detectable phase shift of 0.039 nm (based on 0.9 mV of noise). This corresponds to 1/16,000 of the wavelength of the interrogation beams (632.8 nm). The first experiment to be performed with the LDI system is a study of the laser-spot in the freestream. It is expected that the phase shift due to the thermal spot will be approximately 6.6 nm or 1/96 of the light wavelength, based on a disk-shaped thermal spot with a thickness of 1.5 mm, a pressure matching the freestream static pressure, and a static temperature 100C above the freestream static temperature (which is about 70K). This would yield a signal/noise ratio of about 170; in actuality the signal is probably about ten times smaller, for a signal/noise ratio of the order of 10. An increase in the load resistor to 40 kΩ decreases the detectable-signal limit to 0.02 nm, or about twice the best Smeets reported.

Figure 13 shows the LDI response to a weak acoustic perturbation (soft hand clap). For this test, one of the beams was isolated with a 7 inch long

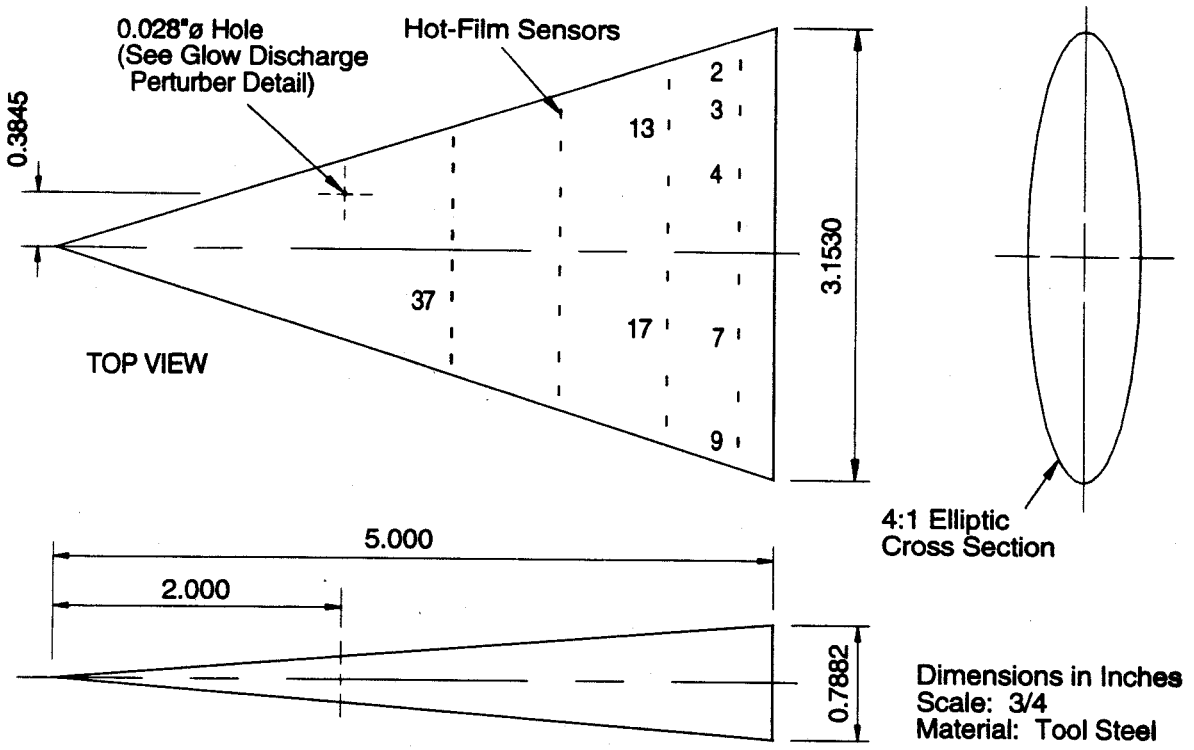

Figure 14: Schematic of Instrumented Elliptic-Cone Model

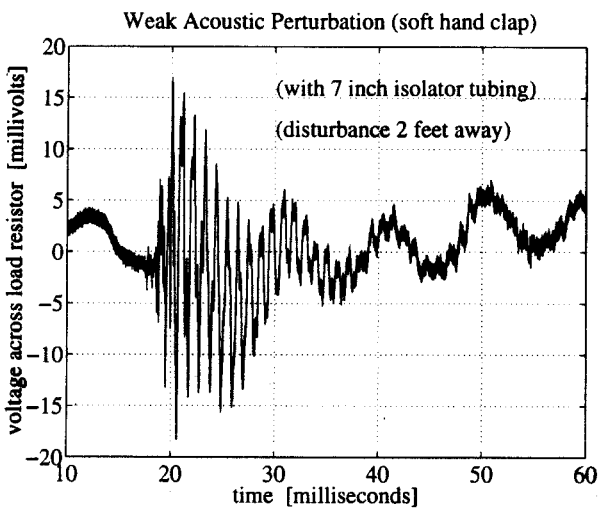

Figure 13: Bench Test of LDI Signal/Noise Ratio

section of brass tubing. Thus, any phase shift in the beam directly outside the isolator tubing, relative to the isolated beam, was detectable, and the LDI essentially became an optical microphone. The 100-Hz noise contained in the signal is approximately 8 mV peak-to-peak, and has been neglected for the signal/noise estimates, for it is presumed to be caused by mechanical vibrations. The LDI is not yet vibrationally isolated.

Stability and Transition Results

Elliptic Cone

A 4:1 aspect-ratio elliptic cross-section cone was machined for the current project (see Figure 14). The 5-inch long cone has a 17.5 degree half-angle in the major axis plane, and a nose diameter of about 0.040 inches. Within available limits of blockage and quiet-Reynolds number, the cone was designed to be as unstable as possible, using computations performed at ASU [41]. Computations performed by Huang and Herbert suggested that the flow would be turbulent 1 inch from the nose, at 1 atm total

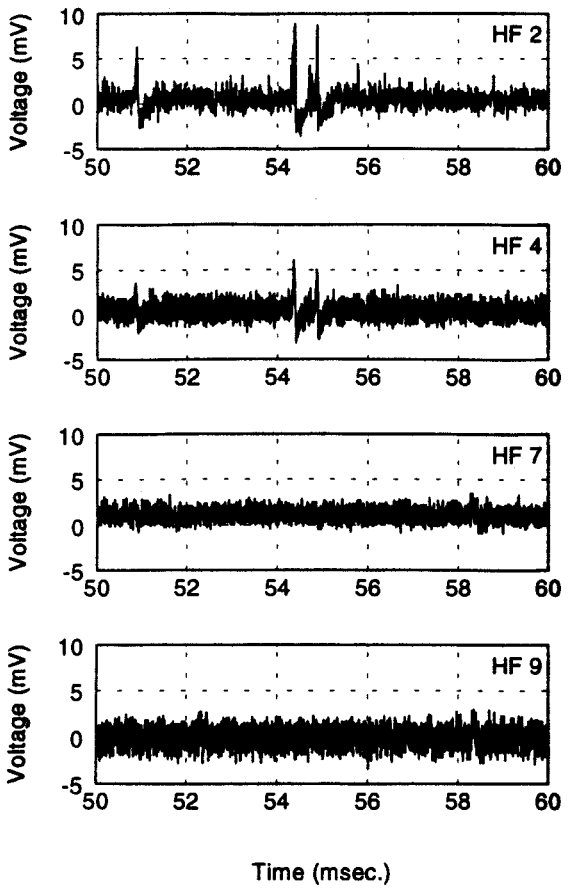

Figure 15: Elliptic-Cone Hot-Film Traces: Run 1

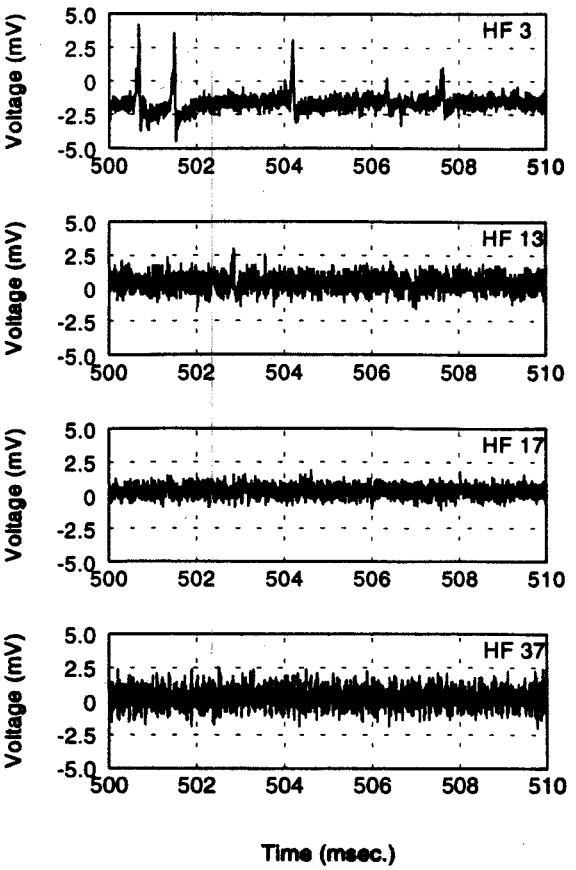

Figure 16: Elliptic-Cone Hot-Film Traces: Run 2

pressure [26]. The model is instrumented with forty custom-built hot-film sensors. Thirty-two hot-film sensors are located on the top or working surface of the model, as shown in Figure 14 by the short dashes. The remaining eight sensors are on the bottom surface.

For the data reported in this study, the hot-films were operated at an over-heat ratio of 1.8. The constant-temperature anemometers used were designed and constructed at Purdue University, and had a frequency response of approximately 20 kHz. The uncalibrated voltage traces are to be used for determining the intermittency and the passage of turbulent spots (as in, for example, references [11] and [56].

Typical hot-film voltage fluctuations near the base of the model are shown in Figures 15 and 16. Four sensors were operated simultaneously; each figure shows data from a separate run. The stagnation pressure was 99.2 kPa and the stagnation temperature 23C. The individual traces are labeled with the hot-film number (e.g. HF 3) which is positioned as shown on Figure 14. Films 7, 9, 17, and 37 are positioned on the 'lower' half of the model (as seen in Figure 14). These traces do not exhibit intermittent behavior; since the noise level is similar to the pre-run noise, they are indicative of laminar flow. Sensors 2, 3, 4, and 13 are located on the 'upper' half of the model. The rare intermittent spikes observed at sensors 2, 3, and 4 are believed to be the signatures of turbulent spots passing the films. Note that time of passage is closely correlated on nearby films. It appears from Figures 15 and 16 that the flow is still laminar at the back of the model, even though this portion is not in the quiet-flow test core. The quiet-flow test core is a 3D shape bounded by Mach lines from the sidewalls; it is 4 inches long only on the centerline. The small intermittency observed on the 'upper' side of the model is believed to be due to the asymmetric positioning of the model in the nozzle. Since the model is positioned diagonally in the near-square cross-section, the 'upper' side is nearer to the flat sidewalls than the 'lower' side, and sees the apparently greater noise radiated from the earlier-transitioning boundary layers on these flat sidewalls.

Hot-wire measurements were also performed on the model, using the same hot-wire anemometer con-

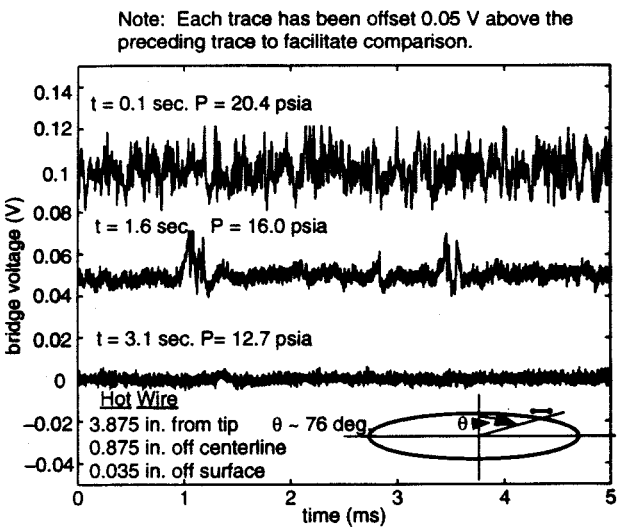

Figure 17: Hot-Wire Traces from Elliptic-Cone Boundary Layer

figuration described earlier. Three segments of data from different periods during a single Ludwieg Tube firing are shown in Figure 17. Next to each trace is shown the estimated stagnation pressure at the time of the segment, calculated using the isentropic expansion model discussed earlier. The initial driver-tube pressure and temperature were 20.75 psia and 80.4 F. The hot wire was located approximately 0.035 in. from the cone surface, 3.875 in. from the cone tip and 0.875 in. from the cone longitudinal centerline. According to the computations of Huang et al. [26], the wire should be within the boundary layer. The corresponding angular position on the cone surface is 76 deg. from the minor axis. The top segment in the figure contains data sampled 0.1 sec. after the beginning of quiet flow in the facility. The voltage has been offset 0.1 volts to facilitate comparison with the other traces. Relatively large fluctuations in the bridge voltage indicate that the flow in the boundary layer is turbulent. Plotted in the center of the figure is data collected 1.6 sec. after the beginning of quiet flow. The voltage has been offset by 0.05 volts. As a result of the decreasing driver-tube pressure during the run, the boundary-layer Reynolds number has decreased and the flow appears to be intermittently turbulent. The lowest trace plotted was collected 3.1 sec. after the beginning of quiet flow. The Reynolds number has decreased even further and from comparison with the pre-run noise the flow appears to be laminar.

In both sets of measurements the cone boundary-layer is laminar under conditions where the local empty-tunnel flow is known to be quiet. The cone boundary-layer becomes intermittent only at locations and pressures where the empty-tunnel flow becomes intermittent. It is thus unclear whether the turbulence observed in the elliptic-cone boundary layer develops naturally or is induced by noise radiated from the nozzle sidewalls. A facility with a higher quiet-flow Reynolds number is needed to resolve the issue, although a more careful characterization of the 3D freestream noise would help.

The data are still useful, however, since PSE calculations for this flow predict that the cone boundary-layer transitions about 1 inch from the model tip [26]. The experimental data *do* clearly show that the boundary layer is laminar well past this position. Huang et al. discuss the many assumptions that were necessary in order to arrive at a non-parallel e^N estimate of the transition location on the model. Although the quiet-flow Reynolds numbers possible in our facility do not allow us to unambiguously determine the quiet-flow transition position on the cone, the data do show that computational improvements are needed.

Hemispherical Nose

Since the current nozzle is quiet only at low Reynolds numbers, receptivity measurements were among the first to be conducted. In particular, the 'blunt-body paradox' is a well-known unresolved problem [45]. Receptivity effects associated with the subsonic region behind the bow shock have been suspected for some time [46], and this issue could be readily investigated in our facility. The resonant effects reported below are broadly similar to those recently computed in 2D blunt-body flows by Zhong [78]. More details can be found in reference [50].

The cylindrical stainless-steel model has a one-inch diameter hemispherical nose that was accurately machined and polished (Figure 18). Since uniform flow starts about 9.3 inches from the throat [64], and the flow remains quiet for about four inches, both the model tip and the shock wave in front of the model were in the uniform quiet-flow region. The shock standoff distance was measured to be approximately 20% of the half-inch radius of the blunt body (0.1 inches) as is shown in Figure 19. An accepted empirical value for a 1/2-inch radius sphere in Mach 4 flow is 0.08 inches [38]. The flow is illustrated in Figure 20 where the extent of the subsonic region has been exaggerated.

An XCQ-062-25A Kulite pressure transducer was used to measure the total pressure behind the shock wave, and was placed inside the model tip,

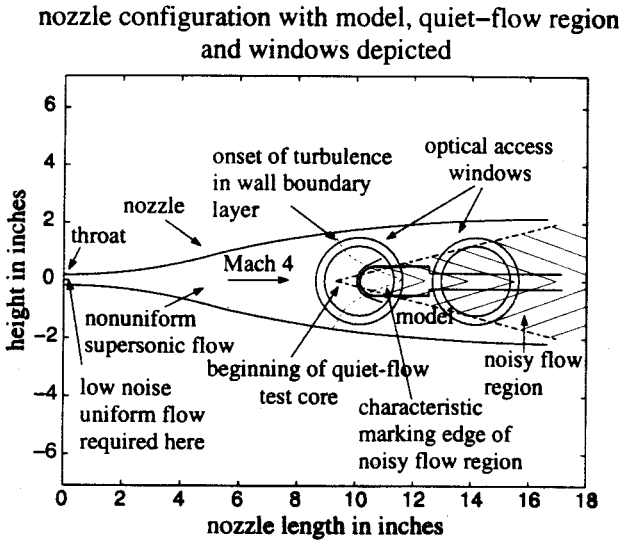

Figure 18: Model in Quiet-flow Region of Test Section

Figure 19: Schlieren Image of Mach-4 Flow

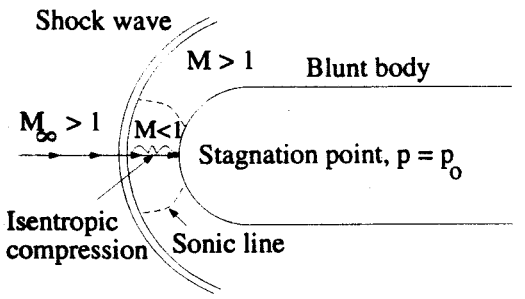

Illustration of Blunt Body in Supersonic Flow

Figure 20: Schematic of Blunt Body in Supersonic Flow.

flush with the nose. The unsteady response of the Kulite was carefully characterized [53]. Originally, the Kulite was approximately 0.006 inches from the tip of the model, with a small hole (0.0032 inches in diameter through the model) in front of the Kulite. However, this limited the frequency response of the system, with the hole acting similar to a low-pass filter. Therefore, spatial resolution was compromised to improve the frequency response of the model and Kulite system. The Kulite pressure transducers are 0.064 inches in diameter.

The laser perturber was used for each run shown here, and the Kulite response was collected at a sampling rate of 2.5 MHz and 250 kHz on two different oscilloscopes. The first oscilloscope was set up in segmented mode with fifty segments, each sampled at 2.5 MHz, and was triggered by the laser firing. The second oscilloscope was unsegmented and was triggered by the start of the tunnel. The streamwise distance between the thermal spot and the model was measured before and after each data set. The total laser energy output was also measured before and after each run.

A single segment from a typical run with Kulite #17 can be seen in Figure 21. The dotted line 'a' marks the electronic noise picked up by the oscilloscope when the laser fires. The dotted line 'b' marks the beginning of the Kulite response to the thermal spot. In this case, the thermal spot was created 20.8 mm upstream of the Kulite pressure transducer. The laser energy was 241 mJ/pulse and the laser fired 0.44 s after the initiation of uniform flow. The

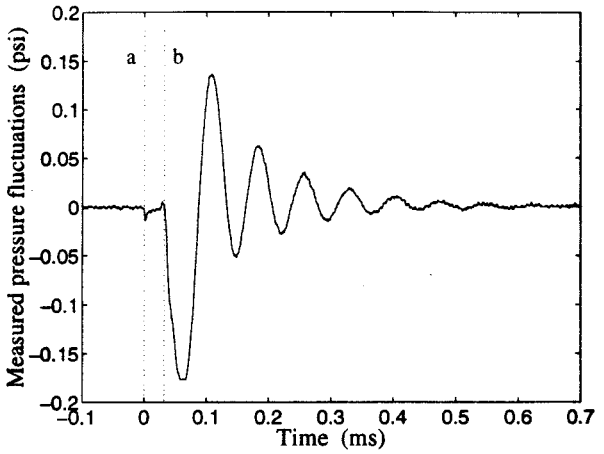

Figure 21: Pressure Fluctuation (Kulite #17) in Response to Laser Perturbation

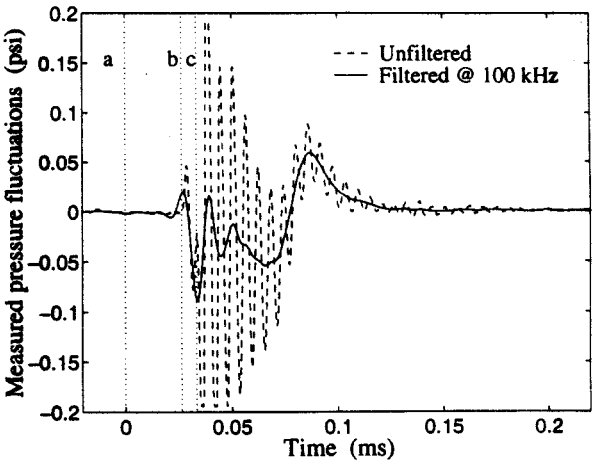

Figure 22: Pressure Fluctuation (Kulite #15) in Response to Laser Perturbation

driver-tube pressure was 14.390 psia and the driver temperature was 77.7°F. The total pressure behind the shock was 2.0 psia initially, according to the normal shock relations. The Kulite started ringing after 31 ± 1 μs (i.e. the time between lines a and b in Figure 21). This agrees well with the theoretical value of 30.7 μs obtained by dividing the distance by the theoretical Mach-4 velocity (675.5 m/s). Thus, the pressure transducer appears to respond to the impact of the thermal spot with the nose of the model.

At first, the pronounced ringing shown in Figure 21 appeared to be clear evidence of a resonant phenomena in the subsonic nose region. Detailed examination of the traces shows a 287 kHz signal riding on the main 13.5 kHz frequency. This higher frequency was at first thought to be the ringing frequency of Kulite #17. The higher frequency remains consistent in each record for this particular run, and it is present for all of the runs with this particular Kulite. However, the mean pressure measured with this Kulite did not match the usual 2.0 psia pitot pressure expected from theory, suggesting that the measurement might be anomalous. Detailed shock tube studies of the Kulite were then performed [53]; these uncovered a different ringing frequency for the Kulite, which performed anomalously and then failed completely.

A resonance frequency associated with the subsonic region behind the shock can be calculated from the maximum width of the subsonic region and the characteristic speed of sound [8]. Using the stagnation-region speed of sound of approximately 340 m/s, about 8.5 kHz results. This is of the same order as the resonance frequency obtained from experimental results.

To determine if the data in Figure 21 are reliable, experiments were conducted with another Kulite pressure transducer of the same model and lot, Kulite #15. In this case, the thermal spot was created 21.1 mm upstream of the model nose. The laser energy was 210 mJ/pulse, and the laser fired 0.76 s after the start of uniform flow. The driver pressure before the run was 14.37 psia and the total temperature was 77.0°F. A typical result with Kulite #15 is shown in Figure 22. Unfortunately, the Kulite ringing seems to be at a substantially higher amplitude than seen previously with Kulite #17. A 4th-order Butterworth digital filter was used to low-pass the data at 100 kHz to eliminate the noise caused by the Kulite ringing. This filtered signal is also shown in Figure 22. The filtered data still seems to show that some ringing of the blunt-nose subsonic region occurs, but the pattern is not as clear.

For this second case, the theoretical shock radius of the thermal spot is approximately 4 mm after 25 μs in the Mach 4 tunnel. For the distance of 21.12 mm, the laser spot should impact with the model nose after 31.5 μs. It is also possible that the Kulite will respond to the shock radiated from the focus of the laser-perturber, if that shock is not sufficiently small to be neglected in this case. Theoretically, the time to shock impact would be 25 μs for the thermal shock. In Figure 22, there may be two

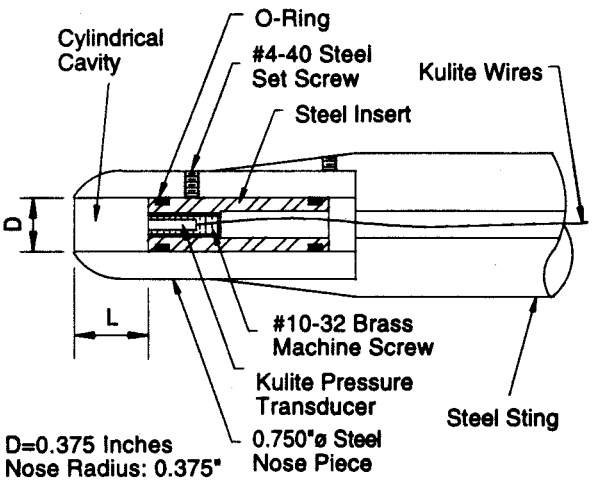

Figure 23: Forward-Facing Cavity Model

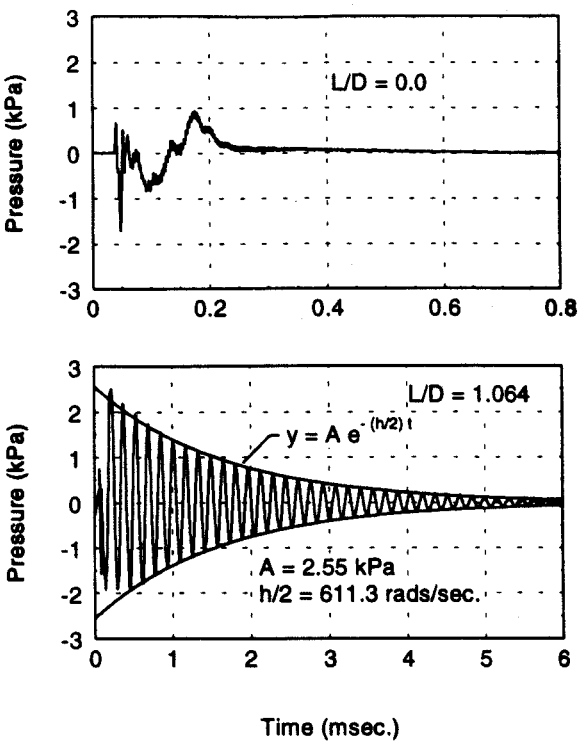

Figure 24: Ringing of Cavity in Response to Thermal Spot

responses to the laser perturbation. The first oscillations begin at 26.5 μs (time between line a and b) and the second begin at 33.5 μs (time between line a and c). It seems possible that with Kulite #15, both the impact of the thermal shock and the thermal spot with the model nose were captured.

In summary, it appears from both experiment and computation that there is some resonant ringing of the subsonic region of the blunt body, but this ringing does not seem to be as clean as that shown in Figure 21, which was probably corrupted somehow by the failing Kulite. The upper part of Figure 24 also shows blunt-body ringing of a sort similar to Figure 22. The data in Figures 22 and 24 are more consistent and seem more reliable. To resolve the ambiguity, the measurements are to be repeated using a hot-wire at the shoulder of the nose, and, later, the differential interferometer.

Forward-Facing Cavity

If a blunt body is modified to add a forward-facing cavity, oscillations can be induced in the cavity which may reduce the heat transfer to the nose. The cavity serves as a resonant amplifier for small disturbances incident from the freestream (see references [76, 16, 33] for details). Although this problem has been studied for some time, we have recently obtained the first quiet-flow measurements of this noise-sensitive flow. The model, shown in Figure 23, consists of a 19.05-mm diameter hemispherically-tipped cylinder, with a flat-face 9.53-mm-diameter cavity (D = 9.53 mm). The cavity depth, L, can be adjusted from zero to about 2 cavity diameters. A Kulite XCQ-062-25A pressure transducer is flush-mounted at the base of the cavity. Under clean quiet-flow conditions, the pressure fluctuations at the cavity base are very low, near the limit of the electronic noise (which is about 0.03% of the pitot pressure). For the cavity depths studied, the cavity behaves like a damped resonant oscillator in response to freestream noise. However, the cavity does seem to amplify freestream fluctuations within the resonant band.

The utility of the laser perturbations was first clearly demonstrated in this flow. The results are summarized in Figure 24, which shows the cavity ringing in response to an incident laser-spot, for two cavity depths. The lower trace shows the damped resonant ringing that is clearly induced in the deeper cavities when the local hot region impinges on the cavity. The upper trace shows the case of zero cavity depth, which is a blunt-body flow similar to the hemispherical nose described above, except that the blunt face is flattened. There is clearly some structure to the response of the subsonic nose region, but clear-cut ringing is not seen. Reference [33] contains the details, including results for cavity depths ranging from 0 to 2 diameters, and results for the damping factor as a function of cavity depth. Re-

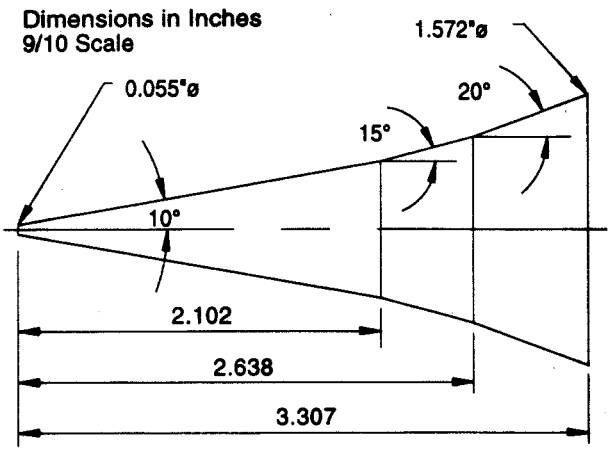

Figure 25: Scale Drawing of Scramjet-Inlet Model

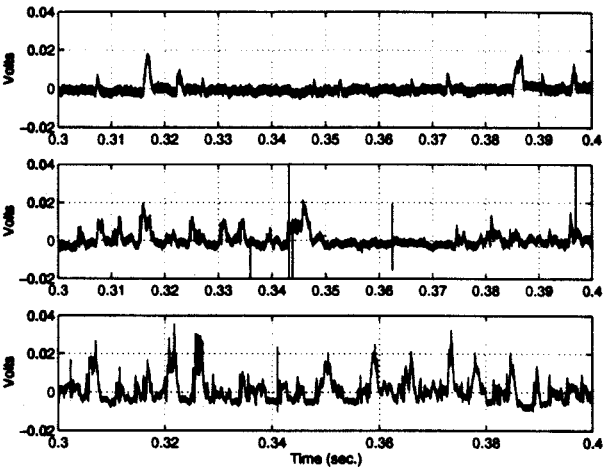

Figure 26: Constant-Temperature Hot-Film Traces on Inlet

cent computations have predicted that the cavity will be self-resonant (have negative damping) when it is very deep [16]. Further quiet-flow experiments are needed to test this prediction.

Scramjet Inlet with Compression Corners

Scramjet engines remain a critical technology for future hypersonic vehicles. Since boundary-layer transition on the inlets affects combustor-inlet flow profiles, separation, and drag, transition is an important factor. An inlet shape similar to those used in the HRE experiments [1] and in Russian designs [79] is being studied at our lab. Figure 25 shows the geometry of interest. The model contains two compression corners designed to induce transition before the boundary-layer enters the combustion chamber (which would be located further aft). To our knowledge, no quiet-flow studies of transition in compression corners have been performed, although some work has been done in conventional wind tunnels [32, 13], and theoretical studies exist [9].

Sixty-four hot-films were fabricated on Kapton sheet by Bartlett's group at Langley, and epoxied to the model. Preliminary studies of the intermittency on the model have been carried out using the anemometers used in reference [56]; more complete studies await the improved anemometers. Figure 26 shows typical results. Three traces are shown; the uppermost is for a film located near the aft portion of the first, 10-degree part of the cone, the middle trace is for a film located between the two compression corners, and the lower trace is for a film located aft of the second compression corner. All three films are positioned along one ray from the vertex. The 0.1-s traces are typical for the complete 1-s records. The intermittency on the first film appears to be less than 10%, while the intermittency on the 2nd film is perhaps 20%, and the intermittency on the aft film is well over 50%. The run was made with a total pressure of 1 atm.

Interpretation of the results is ambiguous because the model is too large to fit completely within the quiet region of the flow at 1 atm. It is possible that the increase in boundary-layer intermittency along the model is due to streamwise increases in the noise radiated from the tunnel wall. However, the increase in intermittency across the second corner is quite sharp, compared to the gradual streamwise increases normally seen in the radiated noise. Our preliminary conclusion is thus that the second corner is effective in tripping the flow. More conclusive results await the completion of the new anemometers described above, and the development of a new nozzle for higher Reynolds-number quiet-flow testing.

Future Plans

Although development of the instrumentation described here can be continued in the existing facility, measurements of stability and transition on realistic models are limited by the low quiet-flow Reynolds numbers that are achievable. A high Reynolds-number 8-inch Mach-6 quiet-flow nozzle is therefore

being designed for the existing tube, with installation currently scheduled for 1998. Plans then call for construction of a larger facility with a 30-inch diameter 200-ft long stainless driver tube, a 24-inch Mach-6 quiet-flow nozzle, and a 12-inch low-noise transonic test section with a solid adaptive wall. Construction of infrastructure for this larger facility is already underway, with completion currently expected around the year 2000 or 2001.

ACKNOWLEDGEMENTS

The work is funded primarily by AFOSR under grants F49620-94-1-0067 and F49620-94-1-0326, monitored by L. Sakell. Funding has also been provided by a gift in memory of K. Hobbie. Much of the funding for tunnel construction and equipment was provided by a gift from the Boeing Company. The blunt-nose receptivity work was funded initially by NASA Langley under Grant NAG-1-1607; after this was terminated Randall was later supported under an Indiana Space Grant Fellowship. The scramjet-inlet work is supported in part by the Hypersonics Program Office at NASA Langley. Langley shop funding provided by the HPO enabled us to obtain the services of Jim Bartlett's highly skilled group, for fabrication and installation of the hot-film arrays. The hot wires are fabricated by George Tennant using designs developed by Tennant, Laufer, and Kendall at JPL. Dr. G. Smeets of the Inst. St.-Louis in France provided many invaluable suggestions and comments; he has generously aided us in duplicating his LDI apparatus. Finally, the mechanical-design and fabrication skills of the AAE machine shop (esp. Don Bower and Joe Zachary) have been invaluable.

REFERENCES

[1] Earl H. Andrews and Ernest A. Mackley. Review of NASA's hypersonic research engine project. Paper 93-2323, AIAA, June 1993.

[2] M. Azzazy, D. Modaress, and T. Hoeft. High-sensitivity density fluctuation detector. *Journal of Physics E: Scientific Instruments*, 20:428–431, 1987.

[3] I.E. Beckwith and C.G. Miller III. Aerothermodynamics and transition in high-speed wind tunnels at NASA Langley. *Annual Review of Fluid Mechanics*, 22:419–439, 1990.

[4] I.E. Beckwith and W.O. Moore III. Mean flow and noise measurements in a Mach-3.5 pilot quiet tunnel. Paper 82-0569, AIAA, 1982.

[5] Defense Science Board. Report of the Defense Science Board task force on the National Aerospace Plane program, November 1992. AD-A274530, 94-00052.

[6] Albert L. Braslow. A review of factors affecting boundary-layer transition. TN D-3384, NASA, August 1966.

[7] D. M. Bushnell. Notes on initial disturbance fields for the transition problem. In M. Y. Hussaini and R.G. Voigt, editors, *Instability and Transition, Volume I*, pages 217–232. Springer-Verlag, 1990. Materials of the workshop held May 15 – June 9,1989 in Hampton, Virginia.

[8] Dennis M. Bushnell. Personal communication, 1995. NASA Langley Research Center, Hampton, Virginia.

[9] K.W. Cassel, A.I. Ruban, and J.D.A. Walker. An instability in supersonic boundary-layer flow over a compression ramp. *Journal of Fluid Mechanics*, 300:265–285, 1995.

[10] F.-J. Chen, M. R. Malik, and I.E. Beckwith. Boundary-layer transition on a cone and flat plate at Mach 3.5. *AIAA Journal*, 27(6):687–693, 1989.

[11] J.P. Clark, P.J. Magari, T.V. Jones, and J.E. LaGraff. Experimental studies of turbulent spot parameters using thin-film heat-transfer gauges. Paper 93-0544, AIAA, January 1993.

[12] S.H. Collicott, S.P. Schneider, and N.L. Messersmith. Review of optical diagnostics for hypersonic low-noise Ludwieg tube facilities. Paper 96-0851, AIAA, January 1996.

[13] Luigi de Luca, Gennaro Cardone, Dominique Chevalerie, and Alain Fonteneau. Viscous interaction phenomena in hypersonic wedge flow. *AIAA Journal*, 33(12):2293–2299, December 1995.

[14] Anthony Demetriades. Stabilization of a nozzle boundary layer by surface heating. Paper 94-2501, AIAA, June 1994.

[15] N. Sam Doughtery and David F. Fisher. Boundary-layer transition correlation on a slender cone in wind tunnels and flight for indications of flow quality. Technical Report

AEDC-TR-81-20, Arnold Engineering Development Center, 1982.

[16] W.A. Engblom, D.B. Goldstein, D. Ladoon, and S.P. Schneider. Fluid dynamics of hypersonic forward-facing cavity flow. Paper 96-0667, AIAA, January 1996.

[17] J.I. Erdos and R. Bakos. Prospects for a quiet hypervelocity shock-expansion tunnel. Paper 94-2500, AIAA, June 1994.

[18] J.M. Floryan. On the Görtler instability of boundary layers. *Progress in Aerospace Sciences*, 28:235–271, 1991.

[19] M. Gaster. A theoretical model of a wave packet in the boundary layer on a flat plate. *Proc. Royal Soc. A*, 347:271–289, 1975.

[20] W.D. Harvey, P.C. Stainback, J.B. Anders, and A.M. Cary. Nozzle wall boundary-layer transition and freestream disturbances at Mach 5. *AIAA Journal*, 13(3):307–314, 1975.

[21] Th. Herbert. Secondary instability of boundary layers. *Annual Reviews of Fluid Mechanics*, 20:487–526, 1988.

[22] Th. Herbert. Boundary-layer transition - analysis and prediction revisited. Paper 91-0737, AIAA, 1991.

[23] Th. Herbert. Parabolized stability equations. In *AGARD Report 793, Special Course on* Progress in Transition Modelling, pages 4/1 – 4/34., 1994.

[24] Uwe G. Hingst. Laminar/turbulent flow transition effects on high speed missile domes. CP 493, AGARD, 1990.

[25] H.G. Hornung and P. Germain. An exploratory study of transition on a slender cone in hypervelocity flow. In R. Kobayashi, editor, *Laminar-Turbulent Transition*, pages 155–162. Springer-Verlag, 1995. Proceedings of the IUTAM Symposium held in Sendai, Japan, September 1994.

[26] Shiling L. Huang, Greg K. Stuckert, and Thorwald Herbert. Cross flow instability of the supersonic flow over a 4:1 elliptic cone. Technical Report 95-0077TR, AFOSR, 1995. AD-A291128.

[27] P.S. Klebanoff and Z.W. Diehl. Some features of artificially thickened fully developed turbulent boundary layers with zero pressure gradient. Technical Note 2475, NACA, 1950.

[28] L. Kleiser and T. Zang. Numerical simulation of transition in wall-bounded shear flows. *Annual Reviews of Fluid Mechanics*, 23:495–537, 1991.

[29] H.A. Korejwo and M.S. Holden. Ground test facilities for aerothermal and aero-optical evaluation of hypersonic interceptors. Paper 92-1074, AIAA, 1992.

[30] A. Kosinov, A. Maslov, and S. Shevelkov. Experiments on the stability of supersonic laminar boundary layers. *J. Fluid Mech.*, 219:621–633, 1990.

[31] A.D. Kosinov, N.V. Seminov, and S.G. Shevelkov. Investigation of supersonic boundary layer stability and transition using controlled disturbances. In *Methods of Aerophysical Research, Proc. 7th International Conference, Novosibirsk, Russia*, pages 159–166, 1994. Volume 2.

[32] A.D. Kosinov and S.G. Shevelkov. Experimental investigation of separation and stability of supersonic laminar boundary layers. In *Separated Flows and Jets*, pages 741–745. Springer-Verlag, 1990. Proceedings of an IUTAM meeting.

[33] Dale W. Ladoon, John D. Schmisseur, and Steven P. Schneider. Laser-induced resonance in a forward-facing cavity at Mach 4. Technical report, AIAA, 1997. Submitted to the Jan. 1997 Aerospace Sciences Meeting.

[34] Dale W. Ladoon and S.P. Schneider. A high frequency glow discharge perturber for supersonic laminar-turbulent transition research. Technical report, Aerospace Sciences Laboratory, School of Aeronautics and Astronautics, Purdue University, West Lafayette, Indiana, 47907-1282, August 1994. 42 pages including 32 figures. Copies can be obtained from the authors.

[35] Dale W. Ladoon and S.P. Schneider. Preliminary tests of a glow discharge perturber in the Purdue quiet-flow Ludwieg tube. Technical report, Aerospace Sciences Laboratory, School of Aeronautics and Astronautics, Purdue University, West Lafayette, Indiana, 47907-1282, June 1995. 15 pages including 6 figures. Copies can be obtained from the authors.

[36] John Laufer. Aerodynamic noise in supersonic wind tunnels. *Journal of Aerospace Sciences*, 28:685–692, 1961.

[37] H. W. Liepmann and A. Roshko. *Elements of Gasdynamics.* John Wiley and Sons, 1957.

[38] H. W. Liepmann and A. Roshko. *Elements of Gasdynamics.* Galcit Aeronautical Series. John Wiley & Sons, Inc., New York, 1957.

[39] H. Ludwieg, Th. Hottner, and H. Grauer-Carstensen. Der rohrwindkanal der aerodynamischen versuchsanstalt Gottingen. In *Sonderdruck aus dem Jahrbuch 1969 der DGLR.* DGLR, 1969.

[40] J. Lukasiewicz. *Experimental Methods of Hypersonics.* Marcel-Dekker, 1973.

[41] Ian J. Lyttle and Helen L. Reed. Use of transition correlations for three-dimensional boundary layers within hypersonic viscous flows. In *Proceedings of the Second Symposium on Transitional and Turbulent Compressible Flows*, August 1995. A joint ASME/JSME Fluids Engineering Conference held at Hilton Head, S.C.

[42] L. M. Mack. Boundary layer linear stability theory. In *Special Course on Stability and Transition of Laminar Flow.* Advisory Group for Aerospace Research and Development, 1984. AGARD Report No. 709.

[43] Mujeeb R. Malik. Prediction and control of transition in supersonic and hypersonic boundary layers. *AIAA Journal*, 27(11):1487–1493, November 1989.

[44] J.A. Masad and A.H. Nayfeh. Laminar flow control of subsonic boundary layers by suction and heat-transfer strips. *Physics of Fluids A*, 4(6):1259–1272, June 1992.

[45] Mark V. Morkovin. Bypass transition to turbulence and research desiderata. In *Transition in Turbines*, pages 161–199, 1985. NASA CP-2386.

[46] M.V. Morkovin. Note on the assessment of flow disturbances at a blunt body traveling at supersonic speeds owing to flow disturbances in free stream. *Journal of Applied Mechanics*, pages 223–229, June 1960.

[47] R. Narasimha. The laminar-turbulent transition zone in the turbulent boundary layer. *Progress in Aerospace Science*, 22:29–80, 1985.

[48] P.G. Parikh and A.L. Nagel. Application of laminar flow control to supersonic transport configurations. Technical Report NASA-CR-181917, NASA, 1990. The authors are with Boeing Commercial Aircraft Company, Seattle, Washington.

[49] E. Piltz. Boundary-layer effects on pressure variations in Ludwieg tubes. *AIAA Journal*, 10:1095–1097, 1972.

[50] Laura A. Randall. Receptivity of a hemispherical nose at Mach 4. Master's thesis, Purdue University, School of Aeronautics and Astronautics, W. Lafayette, Indiana, May 1996.

[51] H.L. Reed and W.S. Saric. Stability of three-dimensional boundary layers. *Annual Review of Fluid Mechanics*, 21:235–284, 1989.

[52] Eli Reshotko. Boundary layer instability, transition, and control. Paper 94-0001, AIAA, 1994. The 1994 Dryden Lecture in Research.

[53] Mario A. Rotea, Laura A. Randall, Ge Song, and Steven P. Schneider. Model identification of a Kulite pressure transducer. In *19th AIAA Advanced Measurement and Ground Testing Technology*, June 1996. AIAA 96–2278.

[54] D.A. Russell, G.S. Knoke, and J.C. Wai. Uniformity of Ludwieg tube flows. In *Modern Developments in Shock Tube Research, Proceedings of the 10th International Shock Tube Symposium, Kyoto*, 1975.

[55] J.D. Schmisseur, S.P. Schneider, T.R. Salyer, and S.H. Collicott. A repeatable laser-generated localized perturbation for application to fluid mechanics. To appear in the Eight International Symposium on Applications of Laser Techniques to Fluid Mechanics, Lisbon, Portugal, July 1996.

[56] J.D. Schmisseur, J.O. Young, and S.P. Schneider. Measurement of boundary-layer transition on the flat sidewall of a rectangular Mach-4 quiet-flow nozzle. Paper 96-0852, AIAA, January 1996.

[57] S. P. Schneider. Improved methods for measuring laminar-turbulent intermittency in boundary layers. *Experiments in Fluids*, 18:370–375, 1995.

[58] S. P. Schneider and C. E. Haven. Quiet-flow Ludwieg tube for high-speed transition research. *AIAA Journal*, 33(4):688–693, April 1995.

[59] S.P. Schneider. A quiet-flow Ludwieg tube for experimental study of high speed boundary

layer transition. Paper 91-5026, AIAA, December 1991. Gives details of design procedures.

[60] S.P. Schneider. A quiet-flow Ludwieg tube for experimental study of high speed boundary layer transition. Paper 92-3885, AIAA, July 1992. Gives detailed design information for facility as constructed.

[61] S.P. Schneider and C. E. Haven. Mean flow and noise measurements in the Purdue quiet-flow Ludwieg tube. Paper 94-0546, AIAA, January 1994.

[62] S.P. Schneider, J.B. McGuire, S.H. Collicott, and T.R. Salyer. Laser-generation of controlled localized perturbations for boundary-layer transition research. In *ICIASF'95 Record: Proceedings of the 16th International Congress on Instrumentation in Aerospace Simulation Facilities*, July 1995. An IEEE meeting held in Dayton, Ohio, IEEE publication number 95CH3482-7.

[63] Steven P. Schneider. Quiet-flow wind tunnels for transition research and testing. A collection of viewgraphs presented at the Third Orbiter Transition Working Group Meeting, NASA Johnson Space Center, Houston, Texas, November 8-9, 1995.

[64] Steven P. Schneider and Christine E. Haven. Mean flow and noise measurements in the Purdue quiet-flow Ludwieg tube. In *AIAA 32nd Aerospace Sciences Meeting and Exhibit*, Reno, Nevada, January 1994. AIAA 94–0546.

[65] Steven P. Schneider, Christine E. Haven, Joseph B. McGuire, Steven H. Collicott, Dale Ladoon, and Laura A. Randall. High-speed laminar-turbulent transition research in the Purdue quiet-flow Ludwieg tube. Paper 94-2504, AIAA, June 1994.

[66] W. Scott. USAF, NASA programs to push hypersonic boundaries. *Aviation Week and Space Technology*, 1996. 6 May issue, p. 22-23.

[67] Ascher Shapiro. *The Dynamics and Thermodynamics of Compressible Fluid Flow.* John Wiley and Sons, 1953.

[68] G. Smeets. Interferometry. Technical Report CO 214/90, Institut Franco-Allemand de Recherches de Saint-Louis, 1990.

[69] G. Smeets and A. George. Investigation of shock boundary layers with a laser interferometer. In *Recent Developments in Shock Tube Research, Proceedings of the Ninth International Shock Tube Symposium, Stanford Univ.*, pages 429–438. Stanford Univ. Press, Stanford, California, 1973.

[70] Ames Research Staff. Equations, tables, and charts for compressible flow. Technical Report Report 1135, National Advisory Committee for Aeronautics, 1952.

[71] K. F. Stetson and R. L. Kimmel. Example of second-mode instability dominance at a Mach number of 5.2. *AIAA Journal*, 30(12):2974–2976, December 1992.

[72] Kwok-On Tong. *On the uniformity of the flow initiated by a non-steady expansion wave.* PhD thesis, University of Washington, 1973.

[73] P.P. Wegener and L.M. Mack. Condensation in supersonic and hypersonic wind tunnels. *Advances in Applied Mechanics*, 5:307–447, 1958.

[74] S. P. Wilkinson, S. G. Anders, and F.-J. Chen. Status of Langley quiet flow facility developments. Paper 94-2498, AIAA, 1994. Presented at the June 1994 Ground Testing Conference.

[75] R.L. Wright and E.V. Zoby. Flight boundary layer transition measurements on a slender cone at Mach 20. Paper 77-719, AIAA, June 1977.

[76] K.B. Yuceil and D.S. Dolling. Nose cavity effects on blunt body pressure and temperatures at Mach 5. *J. Thermophysics and Heat Transfer*, 9(4):612–619, 1995.

[77] Ya. B. Zel'dovich and Yu. P. Raizer. *Physics of Shock Waves and High-Temperature Hydrodynamic Phenomena.* Academic Press, New York, 1966.

[78] X. Zhong. Nonequilibrium effects on the disturbance/bow shock interaction in hypersonic flow past a cylinder. Paper 96-1856, AIAA, June 1996.

[79] V. I. Zvegintsev. Experimental studies of aerodynamic performances of hypersonic scramjet in impulse hot-shot tunnel. Paper 93-2446, AIAA, June 1993.